Scientific Research Publishing

Open Journal of Fluid Dynamics, 2024, 14, 100-122
https://www.scirp.org/journal/ojfd
ISSN Online: 2165-3860
ISSN Print: 2165-3852

Flow and Heat Transfer of a Dusty Williamson MHD Nanofluid Flow over a Permeable Cylinder in a Porous Medium

Oluranti Adejoke Adekanmbi-Akinseye[1], Olugbenga John Fenuga[2], Hamzat Afe Isede[2], Musibau Gbeminiyi Sobamowo[2]

[1]Department of Mathematics, University of Lagos, Lagos, Nigeria
[2]Department of Mechanical Engineering, University of Lagos, Lagos, Nigeria
Email: jokeakinseye55@yahoo.com

How to cite this paper: Adekanmbi-Akinseye, O.A., Fenuga, O.J., Isede, H.A. and Sobamowo, M.G. (2024) Flow and Heat Transfer of a Dusty Williamson MHD Nanofluid Flow over a Permeable Cylinder in a Porous Medium. *Open Journal of Fluid Dynamics*, **14**, 100-122.
https://doi.org/10.4236/ojfd.2024.142005

Received: April 25, 2024
Accepted: June 21, 2024
Published: June 24, 2024

Abstract

This study investigates the flow and heat transfer of dusty Williamson (MHD) Nanofluid flow over a stretching permeable cylinder in a porous medium. Dusty Williamson Nanofluid was considered due to its thermal properties and potential benefits of increasing the heat transfer rate. Firstly, partial differential equations are transformed into coupled non-linear ordinary differential equations through a similarity variables transformation. The resulting set of dimensionless equations is solved analytically by using the Homogony Perturbation Method (HPM). The effects of the emerging parameters on the velocity and temperature profiles as well as skin-friction coefficient and Nusselt number are publicized through tables and graphs with appropriate discussions. The present result has been compared with published papers and found to be in agreement. To the best of author's knowledge, there has been sparse research work in the literature that considers the effect of dust with Williamson Nanofluid and also solving the problem analytically. Therefore to the best of author's knowledge, this is the first time analytical solution has been established for the problem. The results revealed that the fluid velocity of both the fluid and dust phases decreases as the Williamson parameter increases. Motivated by the above limitations and the gaps in past works, therefore, it is hoped that the present work will assist in providing accurate solutions to many practical problems in science, industry and engineering.

Keywords

Williamson, Dusty Particles, Homotopy Perturbation Method (HPM), Magneto Hydrodynamic (MHD), Nanofluid, Porous Medium, Stretching Cylinder

1. Introduction

The study of non-Newtonian fluids has attracted researchers due to its wide variety of applications in engineering, manufacturing processes biomechanics and industry like the extraction of crude oil from petroleum products, Malik *et al.* [1]. A non-Newtonian fluid can be characterized by a viscosity that varies with motion. For non-Newtonian fluids, the viscosity varies with the shear rate. The research on non-Newtonian fluids has received attention because of the limited application of Newtonian fluids. Honey, ketchup, lubrication sprays, and starch, etc., are the examples of non-Newtonian fluids. Amjad [2]. The rheological characteristics of non-Newtonian fluids cannot be explained using the renowned Navier-stokes equations; as a result, various models have been used to describe the properties of non-Newtonian fluid to overcome this deficiency. these models include the Ellis model, Carreus model, power law model, cross model and casson model, etc. The Williamson fluid is one of the most important non-Newtonian fluids characterized by less viscosity with an increase in the rate of shear stress and very similar in its properties of polymeric solutions. Williamson [3] discussed the flow of pseudo plastic materials and discovered a model of Williamson equation to describe the flow of pseudo plastic fluids and experimentally verified the results. Ramesh *et al.* [4] studied Williamson fluid over moving and stationary surfaces with convective boundary conditions. The analysis of Williamson fluid flow over a stretching surface has been conducted by Nadeem *et al.* [5]. A non-Newtonian Williamson boundary layer flow was numerically tackled by using a homotopy analysis method by Khan and Khan [6] The industrial and biological liquids that obey the Williamson fluid are polymers, melts/solution, ketchup, blood, paint, and whipped cream, to mention just a few. Husain *et al.* [7]. Williamson in his theory of pseudo plastic fluid has elaborated the worth of fluid dynamics. It is very important due to its practical implementation in various industries like biological sciences, geophysics, petroleum, chemical industries, and so on Bilal *et al.* [8]. Due to its usefulness, numerous researchers have employed the Williamson model to accurately describe the behavior of fluids throughout the past decade.

Nanofluids are fluids formed by suspending tiny volumes of nanometer-sized particles in base fluids. The traditional heat transfer fluids with low thermal conductivity, such as oil and water, are not able to meet the increasing demand of the more sophisticated heat transfer technologies. To resolve this issue, small solid nanoparticles are added to boost the heat conductivity of these conventional fluids. Choi [9] was the first to investigate and improve the thermal conductivity of fluids. Nanofluids also have an important role in the medical fields, for example, in the use of nanoparticles of gold in the treatment of cancerous tumors, as well as the manufacture of microscopic bombs that are used to eliminate cancerous tumor, Bouslimi [10]. Ashraf *et al.* [11] examined the MHD peristaltic flow of blood-based nanofluid containing nanoparticles, these fluids have significantly influenced the advancement of innovative thermal transportation fluids,

and remarkable efforts have been made in this field in recent years. Tewari-das model was used to model the problem. It is a mathematical model used to describe the thermo physical behaviour of Nanofluids. It was used for this particular model because the velocity and temperature of the fluid and that of the dust particles are the same. The model is a theoretical model that predicts the thermal conductivity of the Nanofluid based on the effective medium approximation (EMA), Tewari and Das [12].

Also, in fluid dynamics, heat and mass transfer play a significant role. Transfer of heat occur when a fluid flows across a surface. The generation of heat is not solely caused by an external heat source, but can also result from frictional forces. There are a lot of applications of heat and mass transfer such as compressor of refrigerator, air conditioner, engine of automobiles and many thermodynamical objects, Nazir *et al.* [13]. The study of fluid flow over a stretching sheet has been a subject of interest in recent years due to its significant importance in areas such as metallurgical processes, polymer extrusion, plastic films, metal spinning, etc. Muzara and Shateyi [14]. The heat transfer of boundary layer flow of non-Newtonian fluids over a stretching cylinder is of great interest to scientists, engineers and researchers because of its extensive range of applications, examples of its applications include the extrusion process, metal extraction, annealing, copper wire thinning, and the pipe industry, Ibrahim and Negera [15]. Kumar *et al.* [16] investigated the two-phase stream of an incompressible liquid with dust particles past a cylindrical geometry stretching at a constant rate. Rashid *et al.* [17] described the heat transfer features of a hybrid nanoliquid and its flow over a stretchy cylinder. Malik *et al.* [18] observed flow of Williamson fluid numerically with heat generation/absorption and variable thermal conductivity effects over a stretched cylinder using Runge Kurta-Fehlberg method. Salahuddin *et al.* [19] considered non-Newtonian fluid flow characteristics utilizing stretching cylindrical surfaces. The effects of heat transportation over stretched cylindrical surfaces are critical in such mechanisms, such as wire drawing, hot rolling and fibre spinning operations. In view of this, numerous researchers have expounded the flow, heat and mass transfers of various kinds of liquids through a stretching cylinder. Umeshaiah *et al.* [20].

The combined effect of heat transfer and temperature across the boundary layer of Nanofluid flows through the porous space in the presence of an external magnetic field is considered an effective means of improving thermal performance. A number of research scholars have been engaged in the fluid dynamics of porous media with different problems. Kothandapani and Srinivas [21] presented magneto hydrodynamic peristaltic transportation and heat transfer under properties of walls action through a porous medium. Gireesha *et al.* [22] focused their attention on the magnetohydrodynamic boundary layer flow and heat transmission embedded in a porous medium.

Magnetohydrodynamics (MHD) is a combination of fluid mechanics and electromagnetism, which defines the behaviour or treatment of a magnetic field

on an electrically conducting fluid and the first to start studying this field, is Alfvén [23]. Wakif and Sehaqui [24] presented the MHD water-based nanofluids with convective boundary conditions. The influence of magnetic fields with constant or varying field strengths, for numerous natural and artificial flows cannot be over-emphasized, whether they are diagonally placed to the direction of flow or inclined at an angle. This is because magnetic fields are important in producing electricity in thermal power stations, heating, magnetic stirring, levitation of molten metals and confinement of some high-temperature electrically conducting pollutants and nuclear wastes in industrial processes.

Dusty fluid model flows have been a subject of particular interest in recent studies due to their two-phase nature. Many researchers worked on the dusty fluid model for various flow configurations and boundary conditions. However, realizing the difficulty of nonlinear coupled equations, no attempt has been made to work out any analytical solution. Although few authors have studied Williamson and nanofluid separately, over-stretching cylinder and plate with a number of publications up to some extent. To the best of the author's knowledge, there has been sparse research work in the literature that considers heat and mass transfer of a dusty Williamson MHD nanofluid flow over a permeable stretching cylinder in a porous medium. Also researchers realized the difficulty of nonlinear coupled equations and have not been able to solve this problem using analytical method. They have always been using numerical methods.

Therefore this is the first time analytical solution is established for the problem. Motivated by the above limitations and the gaps in the past research works, an attempt is made in this study to examine theoretically the problem of boundary layer flows, heat and mass transfer of incompressible, electrically conducting, dusty Williamson MHD nanofluid flow over a permeable horizontally placed stretching cylinder in a porous medium using Tiwari-Das model. The highly non-linear partial differential equations that govern the dusty Williamson Nanofluid flow are reduced into non-linear ordinary differential equations using suitable similarity transformations and then analytically solved using the homotopy perturbation method (HPM). The effects of some chosen pertinent parameters on the fluid velocity, temperature, skin friction coefficient and Nusselt number (heat transfer rate) were displayed using graphs and tables. The results obtained in this current research work were validated by comparing the present results with those from already-published work. An excellent agreement was established. The current research can be employed in a variety of disciplines, including heat engines, heat exchangers, thermocouples, permafrost melting, hot extrusion, oil flow filtration, solar collectors, and many others.

2. Materials and Methods

Consider a steady two-dimensional boundary layer flow of an incompressible viscous dusty Williamson MHD Nanofluid flow over a permeable stretching cylinder in a porous medium which is schematically represented in **Figure 1**.

Magnetic field B_0 is applied normal to the flow along the axis in a radial direction with the assumption of a small Reynolds number so that the induced magnetic field is neglected. T_w and U_w are surface temperature and surface velocity respectively. The ambient fluid temperature and velocity are denoted by T_∞ and U_∞ respectively. Further, w and u are the velocity components in the direction of z and r axis respectively. The dust particles are taken to be small enough and of sufficient number to be treated as continuum and allow concept such as density and velocity to have physical meaning.

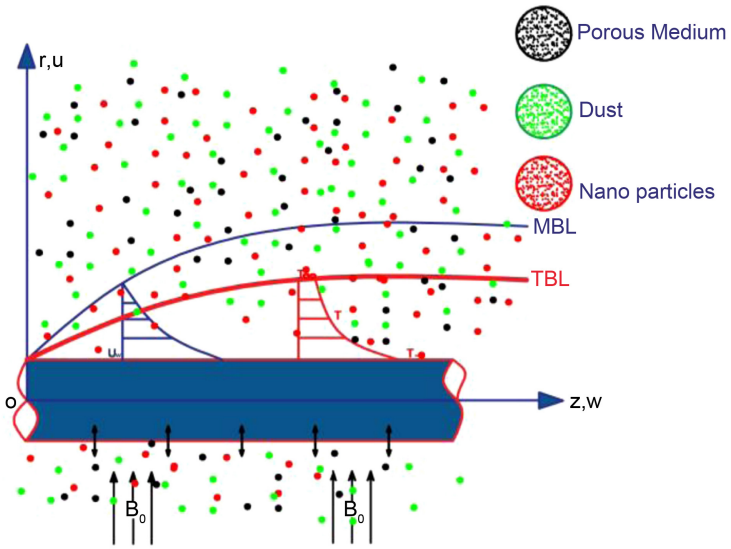

Figure 1. Schematic representation of cylinder boundary-layer flow.

Using the assumptions given above and the well-known boundary layer approximation, the equations governing the heat and mass transfer of dusty Williamson Nanofluid, continuity, momentum, energy, and concentration are specified as follows.

2.1. Continuity Equation

$$\mathbf{div}\boldsymbol{V} = 0 \tag{1}$$

2.2. Momentum Equation

$$\rho\frac{\mathrm{d}V}{\mathrm{d}t} = \nabla\cdot T_0 + \rho b \tag{2}$$

where $\dfrac{\mathrm{d}V}{\mathrm{d}t}$ is the material time derivative. The Cauchy stress tensor τ is given as:

$$\tau = \left[\mu_\infty + \frac{\mu_0 - \mu_\infty}{1-\Gamma_{\dot\gamma}}\right]A_1 \tag{3}$$

The Cauchy stress tensor τ for an incompressible flow is $-p\boldsymbol{I} + \boldsymbol{S}$ in which $\boldsymbol{I}$ is the identity tensor, Here, $\mu_\infty, \mu_0, \Gamma, A_1, \dot\gamma$ corresponds to the viscosity at

infinity, viscosity at zero, positive time constant, first Rivlin-Erickson tensor and shear rate. The shear rate is defined as:

$$\dot{\gamma} = \sqrt{\frac{\chi}{2}}, \tag{4}$$

where

$$\chi = \frac{\text{trace}\left(A_1^2\right)}{2} \tag{5}$$

A_1 = Rivlin-Erickson tensor = $A_1 = L + L^T$;

L = Gradient of the velocity vector L^T = is the transpose of L.

Here we consider only the case for $\mu_\infty = 0$ and $\Gamma_{\dot{\gamma}} < 1$. Now Cauchy stress tensor, τ is reduced to

$$\tau = \left[\frac{\mu_0}{1-\Gamma_{\dot{\gamma}}}\right] A_1 \tag{6}$$

Or, by using binomial expansion to Equation (6), we get

$$\tau = \mu_0 \left[1 + \Gamma_{\dot{\gamma}}\right] A_1 \tag{7}$$

$$A_1 = L + L^{T*}, \tag{8}$$

$L = \nabla \mathbf{v}$ Gradient of the velocity vector $L^{T*} = \left(\nabla \mathbf{v}\right)^{T*}$, the transpose of L;

T^* Represents transpose.

$$\nabla \mathbf{v} = \begin{pmatrix} \frac{\partial u}{\partial r} & \frac{1}{r}\frac{\partial u}{\partial \vartheta} - \frac{v}{r} & \frac{\partial u}{\partial z} \\ \frac{\partial v}{\partial r} & \frac{1}{r}\frac{\partial v}{\partial \vartheta} + \frac{u}{r} & \frac{\partial v}{\partial z} \\ \frac{\partial w}{\partial r} & \frac{1}{r}\frac{\partial w}{\partial \vartheta} & \frac{\partial w}{\partial z} \end{pmatrix} \quad \nabla \cdot \tau = \begin{pmatrix} \frac{\partial \tau_{rr}}{\partial r} + \frac{1}{r}\frac{\partial \tau_{r\vartheta}}{\partial \vartheta} + \frac{\partial \tau_{zr}}{\partial z} + \frac{\tau_{rr} - \tau_{\vartheta\vartheta}}{r} \\ \frac{\partial \tau_{r\vartheta}}{\partial r} + \frac{1}{r}\frac{\partial \tau_{\vartheta\vartheta}}{\partial \vartheta} + \frac{\partial \tau_{z\vartheta}}{\partial z} + \frac{2\tau_{\vartheta r}}{r} \\ \frac{\partial \tau_{rz}}{\partial r} + \frac{1}{r}\frac{\partial \tau_{\vartheta z}}{\partial \vartheta} + \frac{\partial \tau_{zz}}{\partial z} + \frac{\tau_{rz}}{r} \end{pmatrix} \tag{9}$$

In the absence of pressure gradient $T = \tau$. The boundary layer equations that govern the present flow, as per the above assumptions, are listed below as stated by Manjunatha [21].

FLUID PHASE

$$\frac{\partial (ru)}{\partial r} + \frac{\partial (rw)}{\partial z} = 0 \tag{10}$$

$$\begin{aligned} u\frac{\partial w}{\partial r} + w\frac{\partial w}{\partial z} = \nu_{nf}\left(\frac{1}{r}\frac{\partial w}{\partial r} + \frac{\partial^2 w}{\partial r^2}\right) + \nu_{nf}\left[\frac{\Gamma}{\sqrt{2}}\left(\frac{\partial w}{\partial r}\right)^2 + \sqrt{2}\Gamma\frac{\partial w}{\partial r}\frac{\partial^2}{\partial r^2}\right] \\ + \frac{KN}{\rho_{nf}}\left(w_p - w\right) - \left(\frac{\sigma B_0^2}{\rho_{nf}} + \frac{\upsilon_{nf}}{k_p}\right) w \end{aligned} \tag{11}$$

$$\begin{aligned} w\frac{\partial T}{\partial z} + u\frac{\partial T}{\partial r} = \frac{k}{\rho c_P}\left(\frac{1}{r}\frac{\partial T}{\partial r} + \frac{\partial^2 T}{\partial r^2}\right) + \tau\left\{D_B\frac{\partial C}{\partial r}\frac{\partial T}{\partial r} + \frac{D_r}{T_\infty}\left(\frac{\partial T}{\partial r}\right)^2\right\} \\ + \frac{Q_0}{\rho c_P}\left(T - T_\infty\right) \end{aligned} \tag{12}$$

DUST PHASE

$$\frac{\partial\left(ru_p\right)}{\partial r}+\frac{\partial\left(rw_p\right)}{\partial z}=0, \tag{13}$$

$$w_p\frac{\partial w_p}{\partial r}+u_p\frac{\partial w_p}{\partial z}=\frac{K}{\rho}\left(w-w_p\right) \tag{14}$$

$$w_p\frac{\partial T_p}{\partial r}+u_p\frac{\partial T_p}{\partial z}=\frac{Cp_f}{T_tCp}\left(T-T_p\right) \tag{15}$$

Equations (10)-(12) are continuity, momentum and energy equations for the fluid phase and Equations (13)-(15) are for the dust phase, where (w, u) and (w_pu_p) are the velocity components of the nanofluid and dust phases, in the z and r directions respectively. ν, ρ, N, m, K, and k_0 are the kinematic viscosity of the fluid, density of the fluid, number density of the particle phase, mass of the dust particle, Stoke's resistance (drag co-efficient) and permeability of the porous medium respectively, in addition, α represent the thermal diffusivity, ρ refer to density of the fluid. A uniform magnetic field of strength B_0 is applied in the transverse direction of the flow, due to the small magnetic Reynolds number, it is not necessary to introduce the effect of the induced magnetic field.

The associated boundary conditions are as follows

$$w=u_s+U_w\left(z\right),\ u=0,\quad \text{at } r=a, \tag{16}$$

$$w\to\mathcal{U}_e\left(z\right),\quad \text{as } r\to\infty$$

$$w\to 0,\ w_p\to 0,\ \rho_\rho\to\omega_\rho,\quad \text{at } r\to\infty. \tag{17}$$

The following similarity variables are introduced in order to convert the governing equations into the relevant ordinary differential equations (ODEs).

$$\begin{aligned}&\eta=\frac{r^2-a^2}{2a}\sqrt{\frac{\mathcal{U}_w}{\nu z}},\ \psi=a\sqrt{\nu_f\mathcal{U}_wz}\,f\left(\eta\right),\\&\theta=\frac{T-T_\infty}{T_w-T_\infty},\ w=u_w\left(z\right)f'\left(\eta\right),\ u=-\frac{a}{r}\sqrt{\frac{\nu_fu_w}{z}}f\left(\eta\right)\end{aligned} \tag{18}$$

And dust phase:

$$\begin{aligned}&\psi_P=\sqrt[a]{\nu_fu_wz}F\left(\eta\right),\ u_p=-\frac{a}{r}\sqrt{\frac{\nu_fu_w}{z}}F\left(\eta\right),\\&w_p=u_w\left(z\right)F'\left(\eta\right),\ \theta_p\left(\eta\right)=\frac{T_p-T_\infty}{T_w-T_\infty}\end{aligned} \tag{19}$$

ψ Is the stream function is introduced which satisfy the continuity equation, *such that* $u=-\frac{1}{r}\frac{\partial\psi}{\partial r}$ *and* $w=-\frac{1}{r}\frac{\partial\psi}{\partial z}$. η, *f and* θ Aredimensionless transverse distance, dimensionless stream function and dimensionless temperature of the fluid respectively? The kinematic viscosity $\nu=\frac{\mu_\infty}{\rho}$.

It can be confirmed that Equation (10) satisfies the similarity transformations established above in an identical manner. By substituting (18) and (19) into (11)-(16), we obtain the following nonlinear ordinary differential equation

Fluid phase

$$\begin{aligned}&\phi_1\left\{(1+2\gamma\eta)f'''+2\gamma f''\right\}+\phi_1 We(1+2\gamma\eta)^{\frac{1}{2}}\left[\gamma f''^2+2\left\{\gamma f''+(1+2\gamma\eta)f'''\right\}\right]\\&+\phi_2\left(ff''-f'^2\right)-\beta\beta_v\left(f'-F'\right)-\left(\phi_5 Ha+\phi_1 Da\right)f'=0\\&\frac{\phi_1\phi_4}{Pr}\left\{(1+2\gamma\eta)\theta''+2\gamma\theta'\right\}+\phi_1\phi_3\left(\theta' f-2\theta f'\right)\\&+\phi_1\phi_2 Ha\cdot Ec\left(f'\right)^2+\frac{\phi_2\phi_4}{Pr}\left(Af'+B\theta\right)+\phi_1\beta_T\beta\left(\theta_p-\theta\right)=0\end{aligned}\tag{20}$$

Dust phase

$$F'^2-FF''-\beta_v\left(f'-F'\right)=0$$

$$\theta_p' F-2\theta_p F'+\gamma^*\beta_T\left(\theta-\theta_p\right)=0$$

And the corresponding Dimensionless BCs for the prescribed surface temperature (PST)

$$\begin{aligned}&\eta=0,\ \ f=f_w,\ \ f'=1,\ \ \theta=1\\&\eta\to\infty,\ f'=0,\ \ F=f,\ \ F'=0,\ \ \theta=0,\ \ \theta_p=0\end{aligned}\tag{21}$$

Boundary conditions for the prescribed heat flux (PHF)

$$\begin{aligned}&\eta=0,\ \ f=f_w,\ \ f'=\zeta,\ \ \phi_4\theta'=-1\\&\eta\to\infty,\ \ f'=0,\ \ F=f,\ \ F'=0,\ \ \theta=0,\ \ \theta_p=0\end{aligned}\tag{22}$$

The emerging parameters in the dimensionless equations are respectively listed below:

$P_r=\dfrac{\mu c_p}{k}$, is Prandtl number. $Ha=\dfrac{\sigma_f B_0 w}{\rho_f U_f}$ is Hartman/magnetic number;

$\gamma=\dfrac{1}{a}\sqrt{\dfrac{\nu_f z}{u_w}}$ is Curvature parameter, $\beta=\dfrac{z}{ru_w}$, is porosity parameter;

$\delta=h_0\left(\dfrac{2\nu}{U_\infty}\right)^{-1/2}$ is the fluid particle interaction;

$\lambda=\Gamma\sqrt{\dfrac{2u_w}{\nu_{nf}z}}$ is the We is senbergparameter, $S=\dfrac{\nu z}{k_p u_w}$ is the permeability parameter, $Q=\dfrac{\sigma B_0^2}{\rho_{nf}u_w}$ is first order heat source/sink, $R_e=\dfrac{U_w^3(z)}{\nu L}$ is the Reynold's number;

$Ec=\dfrac{u_w z}{Ac_p}$ is Eckert, $Da=\dfrac{u_w}{k_p\rho_f z}$ is Darcy/homogenous porous medium;

$N_t=\dfrac{\tau D_T}{\nu T_\infty}\left(T_w-T_\infty\right)$ is the thermophoresis parameter.

2.3. Parameters of Physical and Engineering Interest for the Problem

The Physical quantities of engineering interest are skin friction coefficient, (C_f)

and Nusselt numbers (*Nu*), which physically indicate the wall shear stress, rate of heat transfer and rate of mass transfer, respectively. They are defined respectively as follows:

Skin friction coefficient, Nusselt number and defined as

$$\left.\begin{aligned} C_f &= \frac{\tau_w}{\rho_{nf} W_w}, \\ Nu_z &= \frac{q_w}{k_f \left(T_w - T_\infty\right)} \end{aligned}\right\} \tag{23}$$

τ_w is the shearing stress and q_w is the heat flux respectively and defined as

$$\begin{aligned} \tau_w &= \mu_{nf} \left[\frac{\partial u}{\partial r} + \frac{\Gamma}{\sqrt{2}} \left(\frac{\partial u}{\partial r} \right)^2 \right]_{r=a} \\ q_w &= -k_{nf} \left. \frac{\partial T}{\partial r} \right|_{r=a} = -k_{nf} \frac{\Delta T r}{a} \sqrt{\frac{U_w}{\nu_f z}} \theta'(\eta) \Big|_{r=a} \end{aligned} \tag{24}$$

Using the dimensionless variables we obtain

$$\left.\begin{aligned} Re_z^{\frac{1}{2}} C_{fz} &= \frac{\phi_1}{\phi_2} \left[f''(0) + Wef''^2(0) \right], \\ Re_z^{-\frac{1}{2}} Nu_z &= -\phi_4 \theta'(0), \end{aligned}\right\} \tag{25}$$

Local Reynold's number $Re_z = \frac{U_w z}{\nu_f}$.

2.4. Method of Solution

Here we employ the use of Homotopy Perturbation Method HPM to obtain the exact analytical solution, this is because the reduced set of similarity equations are coupled and nonlinear in nature, thus it is very difficult to get exact solutions. Here, choosing HPM is very important, because the HPM successfully couples the homotopy theory with the perturbation theory and the main idea is that a complicated problem is continuously deformed into a simple problem which is easy to solve in order to get an analytic exact or approximate solution.

Analysis of the Nonlinear Model Using Homotopy Perturbation Method

Similarly, the governing equation of the model can be transformed to dimensionless forms using the similarity transformation defined (19 and 20) with a little modification in fluid temperature.

Consider a system of nonlinear ordinary differential equations given; there are four equations in total

- Two equations of the fluid phase (Velocity and energy equations).
- Two equations of the dust phase (Velocity and energy equations).

Using homotopy perturbation method to solve velocity equation for the fluid phase mode

$$\begin{aligned}&\phi_1\left\{(1+2\gamma\eta)f'''+2\gamma f''\right\}+\phi_1\lambda(1+2\gamma\eta)^{\frac{1}{2}}\left[\gamma f''^2+2\left\{\gamma f''+(1+2\gamma\eta)f'''\right\}\right]\\&+\phi_2\left(ff''-f'^2\right)-\beta\beta_v\left(f'-F'\right)-\left(\phi_5 Ha+\phi_1 Da\right)f'=0\end{aligned}\tag{26}$$

We rewrite the equations in form that is amendable for ease of analysis

$$\begin{aligned}&\phi_1 f'''+2\phi_1\gamma\eta f'''+2\phi_1\gamma f''+\phi_1 We(1+2\gamma\eta)^{\frac{1}{2}}\gamma f''^2+2\phi_1 We(1+2\gamma\eta)^{\frac{1}{2}}\gamma f''\\&+2\phi_1 We(1+2\gamma\eta)^{\frac{3}{2}}f'''+4\phi_1 We(1+2\gamma\eta)^{\frac{1}{2}}\gamma\eta f'''+\phi_2\left(ff''-f'^2\right)\\&-\beta\beta_v\left(f'-F'\right)-\left(\phi_5 Ha+\phi_1 Da\right)f'=0\end{aligned}\tag{27}$$

and the non linear velocity equations of fluid phase were separated into the Highest linear derivative (L), non linear (N) and remainder (R)

$$L_f(f)=\phi_1 f''',\tag{28}$$

$$N_f(f)=\phi_1 We(1+2\gamma\eta)^{\frac{1}{2}}\gamma f''^2+\phi_2\left(ff''-f'^2\right)\tag{29}$$

$$\begin{aligned}R_f(f)=&2\phi_1\gamma\eta f'''+2\phi_1\gamma f''+2\phi_1 We(1+2\gamma\eta)^{\frac{1}{2}}\gamma f''+2\phi_1 We(1+2\gamma\eta)^{\frac{3}{2}}f'''\\&+4\phi_1 We(1+2\gamma\eta)^{\frac{1}{2}}\gamma\eta f'''-\beta\beta_v\left(f'-F'\right)-\left(\phi_5 Ha+\phi_1 Da\right)f'\end{aligned}\tag{30}$$

The solution of Equation (30) can be assumed to be written as a power series in p

$$f=f_0+pf_1+p^2f_2+p^3f_3+\tag{31}$$

We make assumption of approximating the solution and simplified we arrange the equation and the boundary conditions according to the power of the embedding parameter p, and by Decomposing into zero order, first order and second order.

Solution of Velocity Equation for Fluid Phase for the PST

$$\begin{aligned}\phi_1 f_1'''=&-2\phi_1\gamma f_0''-2\phi_1\gamma\eta f_1'''-\phi_1 We(1+2\gamma\eta)^{\frac{1}{2}}\gamma\left(f_0''\right)^2-2\phi_1 We(1+2\gamma\eta)^{\frac{1}{2}}\gamma f_0''\\&-2\phi_1 We(1+2\gamma\eta)^{\frac{3}{2}}f_0'''-4\phi_1 We(1+2\gamma\eta)^{\frac{1}{2}}\gamma\eta f_0'''-\phi_2\left(f_0 f_0''-\left(f_0'\right)^2\right)\\&+\beta\beta_v\left(f_0'-F_0'\right)+\left(\phi_5 Ha+\phi_1 Da\right)f_0',\end{aligned}\tag{32}$$

Solution of Velocity Equation for Fluid Phase for the PHF

$$\begin{aligned}\phi_1 f_1'''=&-2\phi_1\gamma f_0''-2\phi_1\gamma\eta f_1'''-\phi_1 We(1+2\gamma\eta)^{\frac{1}{2}}\gamma\left(f_0''\right)^2-2\phi_1 We(1+2\gamma\eta)^{\frac{1}{2}}\gamma f_0''\\&-2\phi_1 We(1+2\gamma\eta)^{\frac{3}{2}}f_0'''-4\phi_1 We(1+2\gamma\eta)^{\frac{1}{2}}\gamma\eta f_0'''-\phi_2\left(f_0 f_0''-\left(f_0'\right)^2\right)\\&+\beta\beta_v\left(f_0'-F_0'\right)+\left(\phi_5 Ha+\phi_1 Da\right)f_0'.\end{aligned}\tag{33}$$

3. Results and Discussion

3.1. Computational Verification

Authentication of accuracy of the analytical procedure used was done by comparison, first computations for f'' and θ'' are carried out for Williamson fluid for various values of M and compared with the available published results as shown

in Table 1 and Table 2 and they are establish an excellent agreement.

The accuracy of the result is tested and shown in Table 1, when $\theta'(0)$ was compared with the results of Kumar *et al.* [16] and Manjunatha *et al.* [25] and for different values of Ha, the present results are found in a very good agreement with existing published results. Similarly in Table 2 when $f''(0)$ was compared with the results of Ramesh *et al.* [4], Giresha 22 and Chen [26] the present results are found in a very good agreement. This confirm that the HPM used in this work is perfect and accurate. This proves the validity of the present results, along with the accuracy of the present analytical technique. Therefore, we are confident that our results are highly accurate to analyze this boundary layer flow problem.

Table 1. Comparison of the present results for the dimensionless temperature gradient-$\theta'(0)$ with previous published work of Majunathan *et al.* and Kumar *et al.*

Ha	Kumar *et al.* [16] $-\theta'(0)$	Manjunathan *et al.* [25] $-\theta'(0)$ -$\theta'(0)$	Present study $-\theta'(0)$
0.72	1.0885	1.0885	1.0885
1.00	1.3333	1.3333	1.3333
10.00	4.7969	4.7969	4.7969

Table 2. Comparison of the results of $f''(0)$ for stretching cylinder for various values of Ha with previous published work when $\varphi = \gamma = \lambda = \zeta = M = Pr$.

Ha	Ramesh *et al.* [4] $f''(0)$	Giresha *et al.* [22] $f''(0)$	Chen [26] $f''(0)$	Present study $f''(0)$
0.0	1.000	1.000	1.000	1.000
0.2	1.095	1.095	1.095	1.095
0.5	1.224	1.224	1.224	1.224
1.0	1.414	1.414	1.414	1.414
1.2	1.483	1.483	1.483	1.483
1.5	1.581	1.581	1.581	1.581
2.0	1.732	1.732	1.732	1.732

3.2. Results and Discussion

The exact analytical solution to the governing ODEs (21)-(23) with the boudary conditions (24)-(26) was achieved using the Homotopy Perturbation Method. Graphical illustrations were used to analyze the influences of the pertinent parameters, namely the Curvature parameter, the Magnetic parameter, Prandtl number, Porosity parameter, the Eckert number, Wesseinberg, Fluid particle interaction parameter and the Volume fraction parameter, on respective fluid- and dust-phase. The graphical representation are as follow:

Table 3. Variation of $C_f Re_2^{1/2}$ and $Nu_z Re_2^{-1/2}$ for various values of pertinent parameters (M, β, γ, λ, Ec and Pr) Magnetic (M), fluid particle interaction (β), curvature (γ), Wesseinberg (λ), Eckett (Ec), Prandtl (Pr).

M	β	γ	λ	Ec	Pr	$C_f Re_2^{1/2}$	$Nu_z Re_2^{-1/2}$
0.1	0.1	0.1	0.1	0.1	0.1	0.9385	2.26737
0.3						0.93561	2.26851
0.5						0.93234	2.26872
0.1	0.1					0.99703	2.27093
	0.3					0.96795	2.30030
	0.4					0.93234	2.28734
0.1	0.1	0.2		0.3		0.82409	2.19961
		0.3				0.93234	2.26872
		0.5				0.96953	2.30332
0.1	0.1		0.3			0.98271	2.33303
			0.4	0.5		0.98869	2.35366
				1.0		0.99467	2.38337
				1.0		0.99776	2.41308
					0.5	1.00374	2.44279
					1.0	1.00749	2.44500
					2.0	1.00972	2.44614

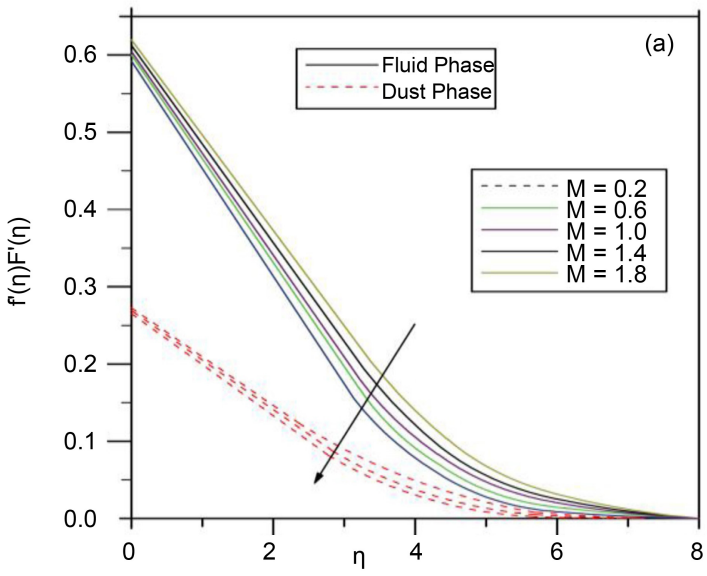

Figure 2. Effect of magnetic number on the fulid and dust phase velocity.

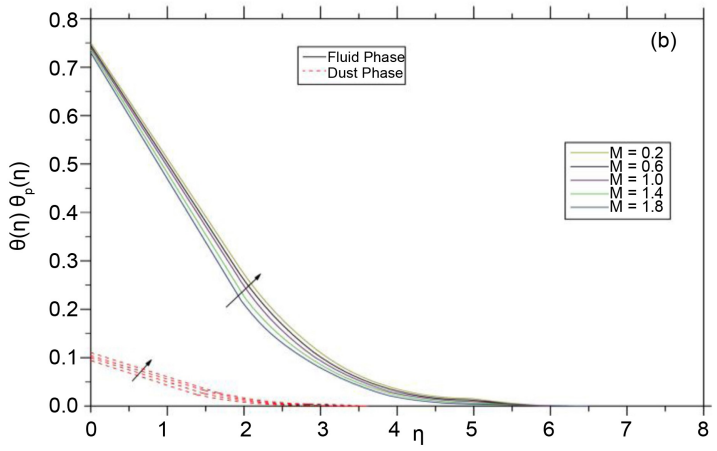

Figure 3. Effect of magnetic number on the fluid and dust phase temperature profiles.

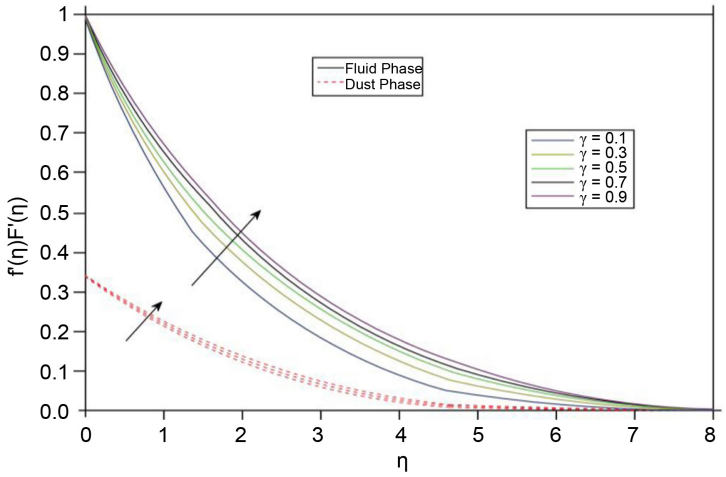

Figure 4. Effect of curvature parameter on the fluid and dust phase velocity profiles.

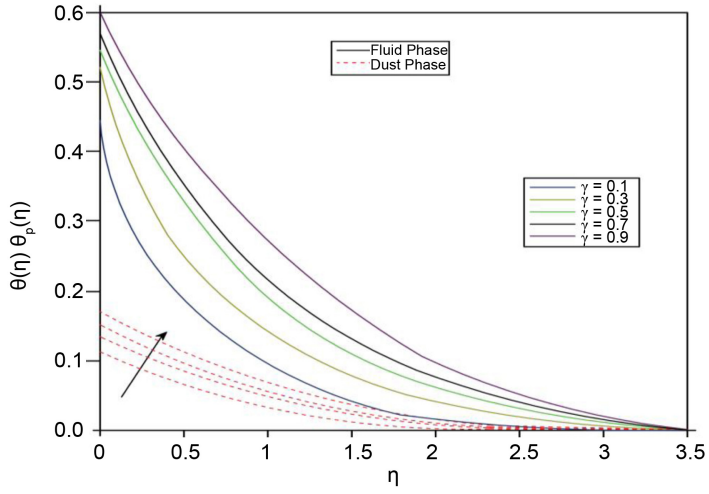

Figure 5. Effect of curvature parameter on the fluid and dust phase temperature profiles.

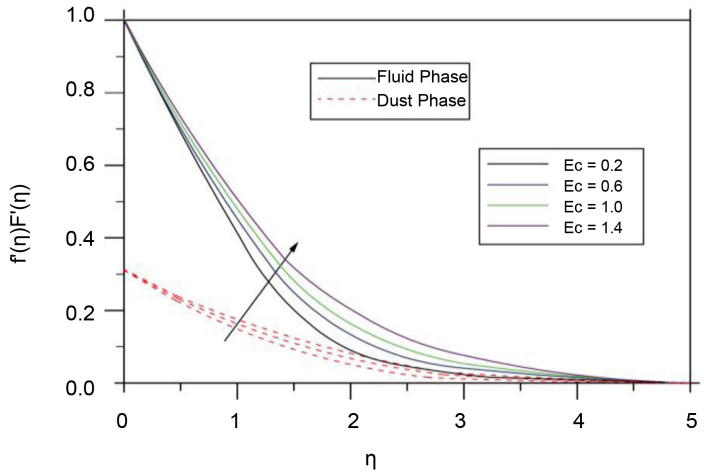

Figure 6. Effect of Eckert parameter on the fluid and dust phase velocity profiles.

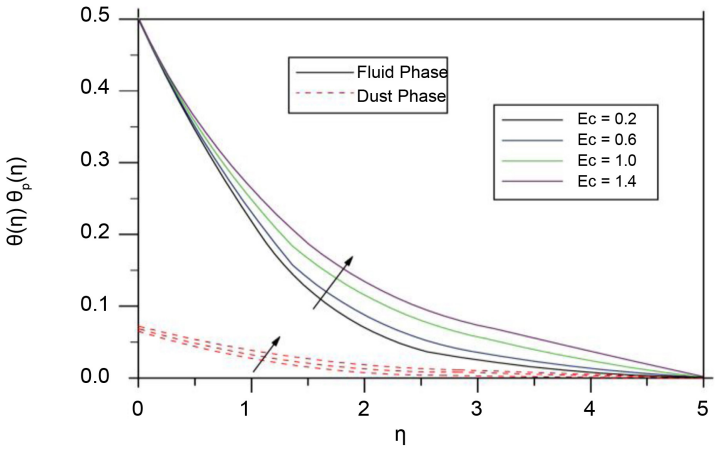

Figure 7. Effect of Eckert parameter on the fluid and dust phase temperature profiles.

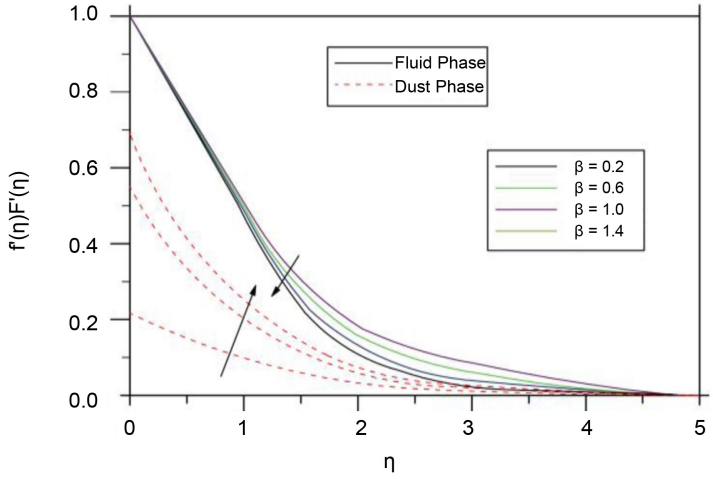

Figure 8. Effect of fluid particle interaction parameter on fluid and dust phase velocity profiles.

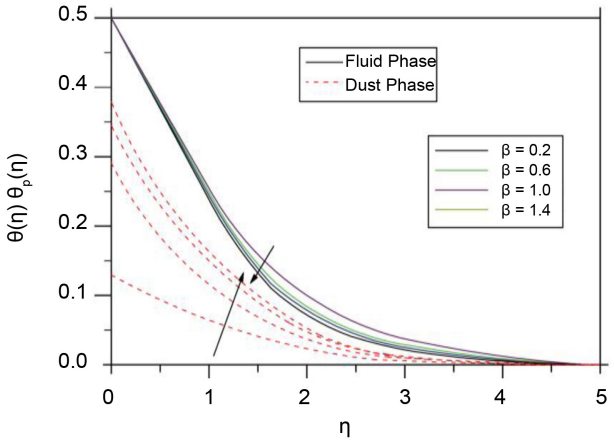

Figure 9. Effect of fluid particle interaction parameter on fluid and dust temperature profiles.

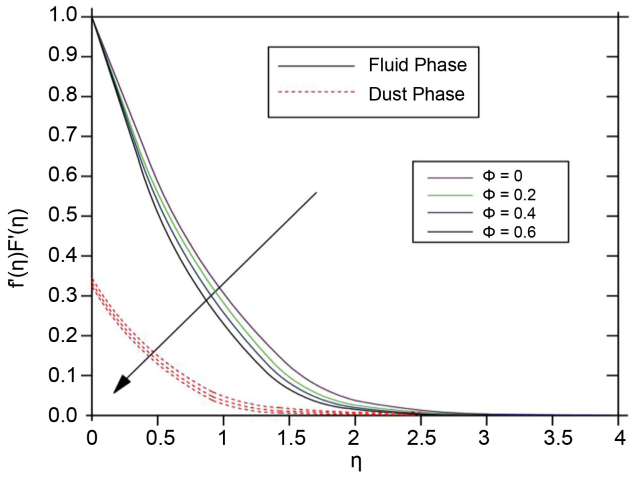

Figure 10. Effect of volume fraction of duct particles on fluid and dust velocity profiles.

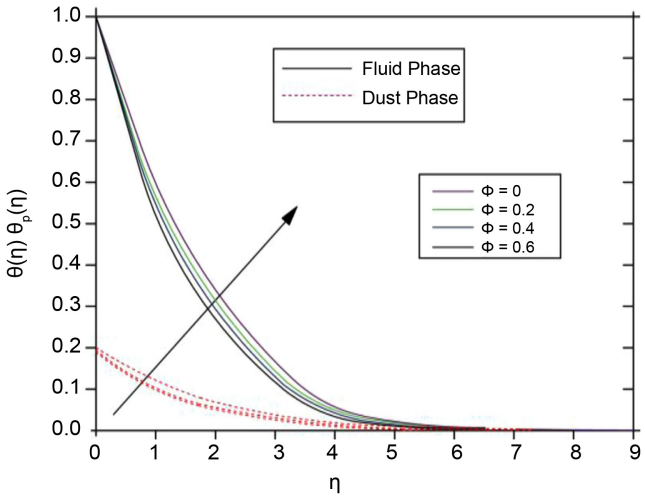

Figure 11. Effect of volume fraction of duct particles on fluid and dust temperature profiles.

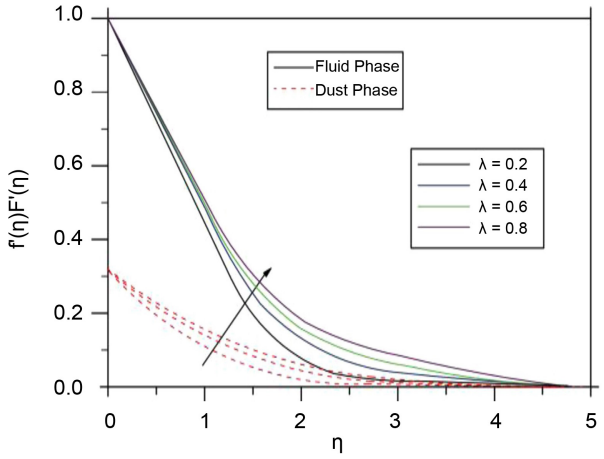

Figure 12. Effect of Wesseinberg parameter on fluid and dust phase velocity profiles.

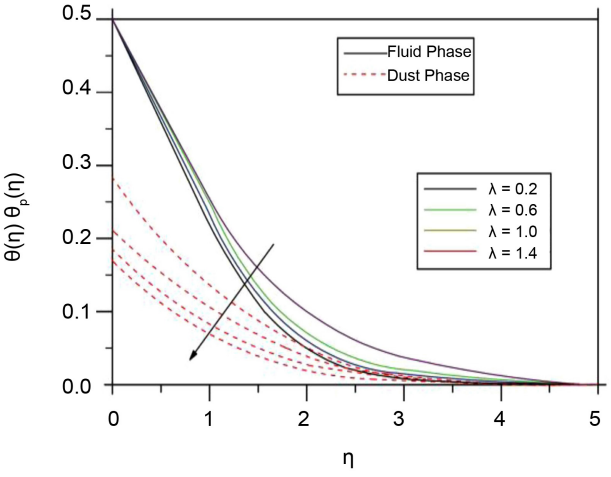

Figure 13. Effect of Wesseinberg parameter on fluid and dust phase temperature profiles.

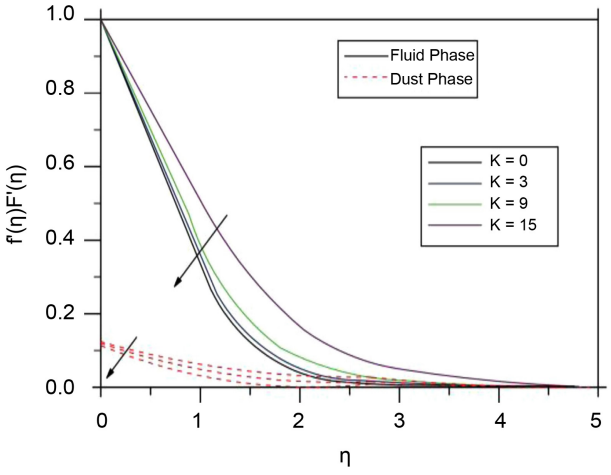

Figure 14. Effect of permeable parameter on fluid and dust phase velocity profiles.

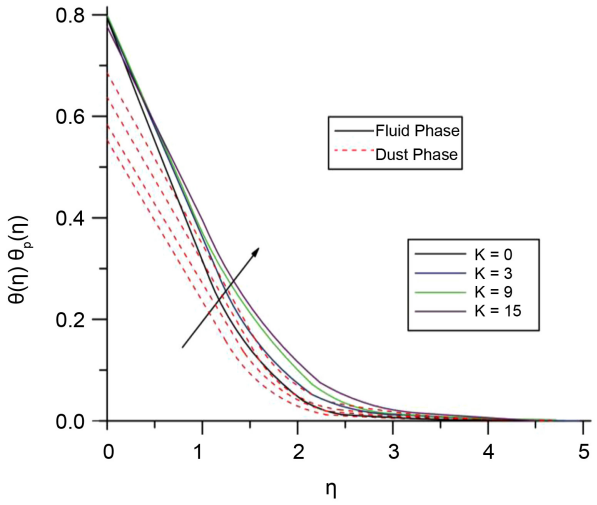

Figure 15. Effect of permeable parameter on fluid and dust phase temperature profiles.

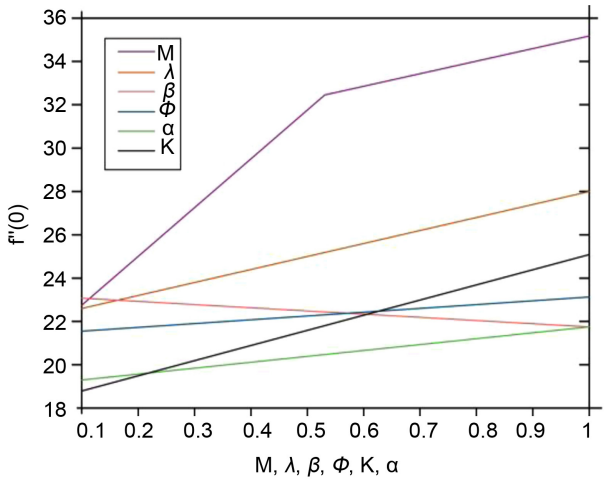

Figure 16. Variation in Skin friction coefficient.

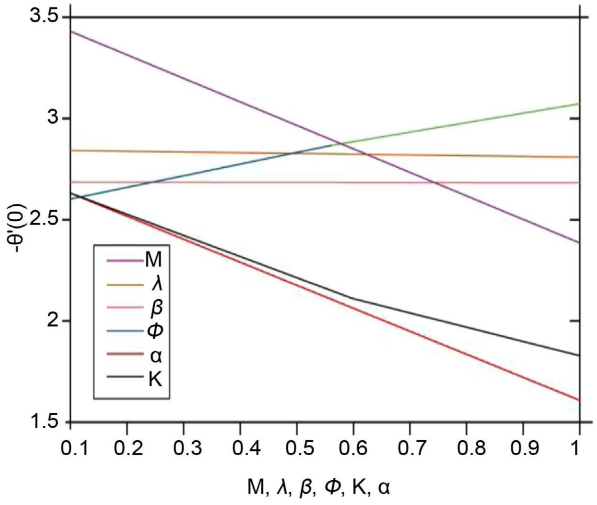

Figure 17. Variation in Nusselt number.

3.3. Influence of Various Parameters on the Velocity and Temperature Profiles

Velocities (f) and (F) as well as, fluid- and dust-phase temperature ($\theta'$and θ_p') are shown in Figures 2-17, Also, the nature of the velocities and temperatures of both phases is examined in this section and an appropriate explanation is provided here. For the analysis of the model Figures 2-17 are plotted for different values of physical parameters. Furthermore, the values of the skin friction coefficient C_{fz} and Nusselt number Nu_z in the presence of the pertinent parameter are shown in Table 3. It is noted that the value of C_{fz} decreases as Wesseinberg λ, volume fraction and fluid particle interaction and increases with Ec. On the other hand, the value of Nu_z decreases with an increase in λ or a decrease in the remaining parameters, as displayed.

Figure 2 and Figure 3 illustrate the effect of the magnetic parameter M on the velocity and temperature distribution of the fluid phase and dust phase respectively. It is clear that higher values of the magnetic parameter M result in a reduction in the fluid and dust phase velocity, along with an elevation in the temperature profiles of both phases. This occurs due to the generation of a resistive drag force, referred to as the Lorentz force, when a transverse magnetic field is applied perpendicular to the flow direction. The force operates in the opposite direction of the flow. This has the effect of reducing the velocity boundary layer and increasing the thickness of the thermal boundary layer. Due to recent observations, we have noticed a rise in the temperature profiles of the flow fluid transport phenomena. With an increase in magnetic parameter M, the momentum boundary layer thickness decreases, leading to a higher velocity gradient.

Figure 4 and Figure 5 illustrate the influence of the curvature parameter, on the velocity and temperature profiles of both fluid and dust particles. With an increase in the curvature parameter, there is a notable enhancement in both the velocity of the fluid phase and the velocity of the dust phase. It is quite evident from Figure 4 that the velocity of the fluid as well as dust phase corresponding to ($\gamma = 0$) is minimum and the increase of (γ) is to increase the velocity within the boundary layer. Moreover ($\gamma = 0$), the problem reduces to flat surface, and hence, the velocity within the boundary layer in the case of cylinder is larger than the flat surface. The presence of a cylinder leads to an increase in the flow rate within the boundary layer compared to a flat surface. This indicates that the increasing speed within the boundary layer is due to expansion in the cylinder size… Consistent with expectations, there is a noticeable increase in both velocity and momentum as we approach the surface of the cylinder. On the other hand, as we move away from the surface, we see a decrease in velocity and momentum, accompanied by an increase in the thickness of the boundary layer. This is because the resistance exerted by the viscous forces near the surface of the cylinder is considerably higher compared to those located further away from it. Furthermore, as the curvature parameter increases, there is a corresponding decrease in the radius of the cylinder. As a result, there is a reduction in the re-

sistance to fluid motion, leading to a subsequent increase in fluid velocity. In the dust phase, the rate of velocity gradient increase is significantly greater in comparison to the fluid phase. An increase in the curvature parameter leads to a significant reduction in the radius of the cylinder, thereby causing a decrease in the resistance to fluid motion. Consequently a decrease in the distribution of heat in both the fluid and dust phases is observed. The data clearly indicates that the temperature profiles of both the fluid and dust phases show an upward trend as the curvature parameter increases.

Figure 6 and Figure 7 show how the Eckert number affects the velocity and temperature distribution of the fluid phase and dust phase, respectively. Just like a mechanical engineer, the graphs clearly show that as the Eckert number Ec increases, the temperature profile also increases. Increases in the Eckert number enhance the intermolecular mobility and kinetic energy within liquids. The thermal variation, with its various stages and the accompanying boundary layer, is further amplified by the intermolecular tension. When the Eckert number (Ec) goes up, there is usually a corresponding increase in the dissipation of energy due to viscosity between particles. The main cause of this phenomenon is that the fluid's viscosity absorbs energy from its motion and transforms it into internal energy, leading to an increase in the fluid's temperature. As a result, the thickness of the thermal boundary layer increases, leading to a higher temperature distribution within the dusty Nanofluid.

The fluid particle interaction parameter β has a significant impact on the velocity and temperature profiles of the fluid and dust phases, Figure 8 and Figure 9. It is worth noting that an increase in the value of β leads to an enhancement in the velocity of the dust phase and a reduction in the velocity of the fluid phase. This phenomenon occurs when there is a strong interaction between the fluid and particle phases, resulting in the particle phase exerting a force that opposes the fluid phase until the particle velocity equals the fluid velocity. It is evident that an increase in the fluid particle interaction parameter leads to an elevation in the temperature profiles of both the fluid and dust phases. This agrees with the general fact that the interaction between the fluid and the particle phase has a greater impact on enhancing the thermal conductivity of the flow than it might otherwise. From Figure 10 and Figure 11, it is clear that an increase in the volume fraction of dust particles leads to a decrease in the velocity profiles of the fluid and dust phases, as well as the temperature profiles. The reason for this phenomenon is that the dust particles take up more space per unit volume of the mixture, resulting in an increase in the mass concentration of the dust phase and a decrease in velocity and thermal boundary layer thickness. The influence of Wesseinberg parameter, λ on velocity and energy profiles in both fluid and dust phases are seen in Figure 12 and Figure 13. The Weissenberg parameter refers to a quantifiable correlation between the rate of fluid flow and a specific duration of the process. The increasing values of the λ lead to an increase in the relaxation time of fluid molecules, so elevating the significance of viscosity and

generating a resistance to the flow of a fluid, ultimately leading to a decrease in velocity of the fluid. The rate of flow and the corresponding increase in boundary layer thickness decrease for the fluid phase and increase for the dust phase as the λ increases. However, the thickening of the temperature boundary layer increases for both the liquid and dust phases as the λ increases. The impact of the permeability parameter on velocity profiles in both the fluid and dust phases is illustrated in Figure 14. The presence of porous medium is observed to cause increased restriction of fluid flow, resulting in slowing down the velocity. Hence, as the permeability parameter increases, there is a corresponding increase in the resistance to fluid motion. Figure 15 demonstrates the impact of increasing values of the permeability parameter on temperature distributions for both the fluid and dust phases. It is evident that higher values of the permeable parameter lead to the thickening of the thermal boundary layer. The influence of non-dimensional governing parameters on the skin friction coefficient for the fluid and dusty phases of Nanofluids is illustrated in Figure 16. The data presented in the figures clearly indicate that an increase in the values of magnetic field parameter, Wesseinberg, mass concentration volume fraction of Nano particles, result in a rise in the skin friction coefficient, while the skin friction coefficient is depreciated as the value of the fluid particle interaction parameter increases. On the other hand the impact of non-dimensional governing parameters on the local Nusselt number can be observed in Figure 17. From the figures, it can be seen that an increase in fluid particle interaction parameter leads to an enhancement in the heat transfer rate in both fluid and dust phases. However, an increase in the magnetic field parameter, Wesseinberg, parameter, mass concentration of dust particles and volume fraction of Nano particles, leads to a decrease in the heat transfer rate.

4. Conclusion

This study examines the flow of a two-dimensional Williamson MHD Nanofluid over a stretching permeable cylinder immersed in a porous medium. The mathematical equations of this two-phase flow model are solved by using the Homotopy perturbation Method on the Matlab software. The work graphically presents and discusses the impacts of various governing parameters on the velocity and temperature profiles, as well as the skin friction coefficient and Nusselt number. The main findings of this investigation are as follows:

- Increasing values of Magnetic field parameter M decreases the velocity profile as well as the momentum boundary layer thickness and increases temperature profile of the fluid.
- The velocity of the fluid and dust phases rises as the curvature parameter was increased. Similar patterns were noted in the temperature profiles of both phases.
- The temperature profile for both the fluid and dust phases improves as the Eckert number increases.

- Increasing the fluid particle interaction β decreased the velocity of fluid phase and increased the velocity of dust phase and a rise in β, increased the temperature of the fluid phase and decreased the temperature of the dust phase.
- Increasing the volume fraction of the dust particles results in a reduction in the velocity profiles and enhances the temperature profiles of both phases.
- Increasing the Wesseinberg, fluid particle interaction and the porosity parameter improves the Nusselt (heat transfer rate) and reduces the skin friction coefficient.
- Magnetic field parameter has the tendency to reduce the skin friction coefficient and Nusselt number.
- An increase in magnetic field parameter and porosity parameters contributes to a gradual decrease in the skin friction coefficient.

5. Contributions to Knowledge

The following contributions are made in advancement of the body of knowledge:

The uniqueness of this current study is the addition of dust to Williamson nanofluid. Also, researchers realized the difficulty of nonlinear coupled equations and have not been able to solve this problem using analytical method, they have always use numerical method. Nobody has approached the problem analytically. Therefore this is the first time analytical solution is established for the problem. Also the study revealed that dusty particles and nanoparticles contributed significantly to reducing temperature profiles and this can be researched further to be a coolant in larger engineering industries. Motivated by the above limitations and the gaps in past works, therefore, it is hoped that the present work will assist in providing accurate solutions to many practical problems in science, industry and engineering.

Acknowledgements

The authors are grateful to the authors referred to in this work.

Conflicts of Interest

The authors declare no conflicts of interest.

References

[1] Malik, M.Y. and Salahuddin, T. (2015) Numerical Solution of MHD Stagnation Point Flow of Williamson Fluid Model over a Stretching Cylinder. *International Journal of Nonlinear Sciences and Numerical Simulation*, **16**, 161-164. https://doi.org/10.1515/ijnsns-2014-0035

[2] Amjad, M., Ahmed, I., Ahmed, K., Alqarni, M.S., Akbar, T. and Muhammad, T. (2022) Numerical Solution of Magnetized Williamson Nanofluid Flow over an Exponentially Stretching Permeable Surface with Temperature Dependent Viscosity and Thermal Conductivity. *Nanomaterials*, **12**, Article 3661. https://doi.org/10.3390/nano12203661

[3] Williamson, R.V. (1929) The Flow of Pseudoplastic Materials. *Industrial & Engi-*

neering Chemistry, **21**, 1108-1111. https://doi.org/10.1021/ie50239a035

[4] Ramesh, G.K., Gireesha, B.J. and Bagewadi, C.S. (2012) Heat Transfer in MHD Dusty Boundary Layer Flow over an Inclined Stretching Sheet with Non-Uniform Heat Source/Sink. *Advances in Mathematical Physics*, **2012**, Article 657805. https://doi.org/10.1155/2012/657805

[5] Nadeem, S., Hussain, S.T. and Lee, C. (2013) Flow of a Williamson Fluid over a Stretching Sheet. *Brazilian Journal of Chemical Engineering*, **30**, 619-625. https://doi.org/10.1590/s0104-66322013000300019

[6] Khan, N.A. and Khan, H. (2014) A Boundary Layer Flows of Non-Newtonian Williamson Fluid. *Nonlinear Engineering*, **3**, 107-115. https://doi.org/10.1515/nleng-2014-0002

[7] Hussain, F., Hussain, A. and Nadeem, S. (2020) Thermophoresis and Brownian Model of Pseudo-Plastic Nanofluid Flow over a Vertical Slender Cylinder. *Mathematical Problems in Engineering*, **2020**, Article 8428762. https://doi.org/10.1155/2020/8428762

[8] Bilal, M., Siddique, I., Borawski, A., Raza, A., Nadeem, M. and Sallah, M. (2022) Williamson Magneto Nanofluid Flow over Partially Slip and Convective Cylinder with Thermal Radiation and Variable Conductivity. *Scientific Reports*, **12**, Article No. 12727. https://doi.org/10.1038/s41598-022-16268-2

[9] Choi, S.U. and Eastman, J.A. (1995) Enhancing Thermal Conductivity of Fluids with Nanoparticles. *ASME International Mechanical Engineering Congress & Exposition*, San Francisco, 12-17 November 1995, 99-106.

[10] Bouslimi, J., Omri, M., Mohamed, R.A., Mahmoud, K.H., Abo-Dahab, S.M. and Soliman, M.S. (2021) MHD Williamson Nanofluid Flow over a Stretching Sheet through a Porous Medium under Effects of Joule Heating, Nonlinear Thermal Radiation, Heat Generation/Absorption, and Chemical Reaction. *Advances in Mathematical Physics*, **2021**, Article 9950993. https://doi.org/10.1155/2021/9950993

[11] Yasmin, A., Ali, K. and Ashraf, M. (2020) Study of Heat and Mass Transfer in MHD Flow of Micropolar Fluid over a Curved Stretching Sheet. *Scientific Reports*, **10**, Article No. 4581. https://doi.org/10.1038/s41598-020-61439-8

[12] Tiwari, R.K. and Das, M.K. (2007) Heat Transfer Augmentation in a Two-Sided Lid-Driven Differentially Heated Square Cavity Utilizing Nanofluids. *International Journal of Heat and Mass Transfer*, **50**, 2002-2018. https://doi.org/10.1016/j.ijheatmasstransfer.2006.09.034

[13] Nazir, S., Kashif, M., Zeeshan, A., Alsulami, H. and Ghamkhar, M. (2022) A Study of Heat and Mass Transfer of Non-Newtonian Fluid with Surface Chemical Reaction. *Journal of the Indian Chemical Society*, **99**, Article 100434. https://doi.org/10.1016/j.jics.2022.100434

[14] Muzara, H. and Shateyi, S. (2023) Magnetohydrodynamics Williamson Nanofluid Flow over an Exponentially Stretching Surface with a Chemical Reaction and Thermal Radiation. *Mathematics*, **11**, Article 2740. https://doi.org/10.3390/math11122740

[15] Ibrahim, W. and Negera, M. (2020) The Investigation of MHD Williamson Nanofluid over Stretching Cylinder with the Effect of Activation Energy. *Advances in Mathematical Physics*, **2020**, Article 9523630. https://doi.org/10.1155/2020/9523630

[16] Kumar, K.G., Rudraswamy, N.G., Gireesha, B.J. and Manjunatha, S. (2017) Non Linear Thermal Radiation Effect on Williamson Fluid with Particle-Liquid Suspension Past a Stretching Surface. *Results in Physics*, **7**, 3196-3202. https://doi.org/10.1016/j.rinp.2017.08.027

[17] Rashid, M., Ansar, K. and Nadeem, S. (2020) Effects of Induced Magnetic Field for Peristaltic Flow of Williamson Fluid in a Curved Channel. *Physica A*: *Statistical Mechanics and Its Applications*, **553**, Article 123979. https://doi.org/10.1016/j.physa.2019.123979

[18] Malik, M.Y., Bibi, M., Khan, F. and Salahuddin, T. (2016) Numerical Solution of Williamson Fluid Flow Past a Stretching Cylinder and Heat Transfer with Variable Thermal Conductivity and Heat Generation/absorption. *AIP Advances*, **6**, Article 035101. https://doi.org/10.1063/1.4943398

[19] Malik, M.Y. and Salahuddin, T. (2015) Numerical Solution of MHD Stagnation Point Flow of Williamson Fluid Model over a Stretching Cylinder. *International Journal of Nonlinear Sciences and Numerical Simulation*, **16**, 161-164. https://doi.org/10.1515/ijnsns-2014-0035

[20] Umeshaiah, M., Madhukesh, J., Khan, U., Rana, S., Zaib, A., Raizah, Z., *et al*. (2022) Dusty Nanoliquid Flow through a Stretching Cylinder in a Porous Medium with the Influence of the Melting Effect. *Processes*, **10**, Article 1065. https://doi.org/10.3390/pr10061065

[21] Kothandapani, M. and Srinivas, S. (2008) On the Influence of Wall Properties in the MHD Peristaltic Transport with Heat Transfer and Porous Medium. *Physics Letters A*, **372**, 4586-4591. https://doi.org/10.1016/j.physleta.2008.04.050

[22] Gireesha, B.J., Roopa, G.S. and Bagewadi, C.S. (2012) Effect of Viscous Dissipation and Heat Source on Flow and Heat Transfer of Dusty Fluid over Unsteady Stretching Sheet. *Applied Mathematics and Mechanics*, **33**, 1001-1014. https://doi.org/10.1007/s10483-012-1601-9

[23] Alfvén, H. (1942) Existence of Electromagnetic-Hydrodynamic Waves. *Nature*, **150**, 405-406. https://doi.org/10.1038/150405d0

[24] Wakif, A., Boulahia, Z., Amine, A., Animasaun, I.L., Afridi, M.I., Qasimd, M., *et al*. (2018) Magneto-Convection of Alumina-Water Nanofluid within Thin Horizontal Layers Using the Revised Generalized Buongiorno's Model. *Frontiers in Heat and Mass Transfer*, **12**, 1-15. https://doi.org/10.5098/hmt.12.3

[25] Manjunatha, P.T., Gireesha, B.J. and Prasannakumara, B.C. (2014) Thermal Analysis of Conducting Dusty Fluid Flow in a Porous Medium over a Stretching Cylinder in the Presence of Non-Uniform Source/Sink. *International Journal of Mechanical and Materials Engineering*, **9**, Article No. 13. https://doi.org/10.1186/s40712-014-0013-8

[26] Chen, C. (2009) Magneto-Hydrodynamic Mixed Convection of a Power-Law Fluid Past a Stretching Surface in the Presence of Thermal Radiation and Internal Heat Generation/Absorption. *International Journal of Non-Linear Mechanics*, **44**, 596-603. https://doi.org/10.1016/j.ijnonlinmec.2009.02.004